Simulations of linear and branched actin networks with formin and arp 2/3 complex as mediators

Ondrej Maxian

May 17, 2024

1   Introduction

A great mystery in cell biology is how cells mediate the assembly of different cytoskeletal structures at different times in the cell cycle. One important example of this is branched vs. linear actin filament networks. When cells migrate, they form a branched network at their leading edge, which can be important for stable adhesion to a substrate. On the other hand, when cells divide, they form a contractile ring of linear actin filaments. The unidirectional (non-branched) nature of the ring is vital to transmit force in the correct direction for the completion of cytokinesis [1].

While it is clear that different network architectures are required for different cellular functions, the molecular mechanisms by which cells control the assembly of branched vs. linear actin structures are still incompletely understood. At the most basic level, linear actin filaments can assemble in two ways: via formin-mediated assembly, and via spontaneous nucleation [1, 24]. Seeing as spontaneous nucleation is energetically unfavorable, formin can significantly speed up filament nucleation [27] to the point where it dominates assembly dynamics. This is also the case in the presence of profilin [28], which can block the spontaneous nucleation of filaments, thereby causing filament assembly to be dependent on formin [1, 25].

Branched actin networks are dependent on a different assembly factor called the arp 2/3 complex. While this complex can aid in nucleation of linear filaments, assembly is most efficient when it binds to an existing "mother" filament. The fixed binding angle of arp 2/3 complex (typically around 70 degrees) causes the formation of tree-like branched actin networks [24, 1]. Because the arp 2/3 complex fixes the minus end of the "daughter" filament onto the mother, the branches can only grow from their plus ends, and thus branched structures do not exhibit treadmilling and are typically more stable than their linear counterparts [1, 20, 15]. Unlike formin networks, whose

growth is aided by the presence of profilin, arp 2/3-complex-mediated growth is *inhibited* by profilin, which blocks the association of an arp 2/3 activator (WASP VCA) with monomeric actin, a step which is necessary for branch formation [31].

While the key molecular players in branched vs. linear network formation are by now well understood, there is still some debate over exactly *how* the cell might program the actin to polymerize into one type of structure vs. the other. In the simplest case when there is exactly one structure formed, the kinetics become quite simple: the elongation rate is proportional to a constant times the amount of available (free) actin monomers [32], and the dissociation rate is constant. Solving the simple equation $k_{on}C = k_{off}$ gives an equilibrium concentration (about 0.1 μM) at which the structure assumes a steady state size. But introducing multiple structures (either of the same kind or of different types), throws off this balance, as actin assembly kinetics alone do not provide a mechanism for controlling the size (length) or type (linear vs. branched) of multiple actin structures, instead only setting the total amount of actin incorporated [19]. To control this, the conventional viewpoint is that external or internal signals [6] activate signaling cascades which eventually cause the cell to produce more or less of a particular type of network [16, 24, 32].

Yet recent experiments have demonstrated that a limiting actin pool, interacting with actin binding proteins, must also play a part in determining the types of structures produced [5, 32, 7, 34, 35]. In general, these experiments have demonstrated *in vivo* steady states in a variety of organisms, all characterized by linear/branched actin structure ratios that are set by the concentration ratio of actin, formin, arp 2/3 complex, and profilin. For instance, in budding yeast cells, reducing the amount of actin (at constant concentration of the other proteins) led to more linear networks, while increasing the amount of actin led to more branched networks. Other experiments using arp 2/3 complex inhibitors [5] suggested that the release of F-actin via disassembly is important for the assembly of new structures [32], and that the occupation of monomers in existing branched structures limits the amount of linear filaments that can be created. They also demonstrated that there might be a quasi-steady state that is stable on relevant biological timescales (minutes to hours) where structures with different growth rates can coexist [12, 33]. This intermediate-timescale regime was the focus of a recent simulation study on linear filaments [2], which found that spontaneous nucleation of actin filaments gives rise to a quasi-stable, near-uniform length distribution.

In this paper, we combine simulations and in vitro experiments to understand if a minimal set of known interactions between actin, formin, arp 2/3 complex, and profilin can reproduce the results previously observed *in vivo* about the distribution of branched vs. linear actin networks.

Unlike previous simulation studies, which focus on linear filaments with at most two other proteins [9, 17, 3, 26, 18], here we develop a simulation framework that can account for an arbitrary number of barbed-end binding proteins (formin, capping protein, etc.) and monomer-sequestering proteins (profilin, thymosin $\beta4$, etc) in the presence of a single branching protein (arp 2/3 complex). By modeling branched and linear networks with the relevant actin binding proteins, and using rates from the literature to specify the kinetics, we obtain a picture of how a limiting actin pool alone can give rise to different network architectures. The observations we make in simulations can then be used to design *in vitro* experiments that test whether the mechanisms we identify are actually borne out in practice.

With this general program in mind, the specific outline of this paper is as follows. Section 2 summarizes the algorithm we use for simulations, which is relatively standard but informed by the most complete picture of spontaneous nucleation developed in [27]. Section 3 focuses on linear filament assembly, which has been explored extensively in previous work (e.g., [9, 3]). Because of this, we confine most of our results to the appendix, with the main text giving only the necessary information that sets the stage for branching, which we study in Section 3.2. Our simulations on branching show how a high arp 2/3 concentration can siphon actin monomers into branches, dropping the density of linear filaments in the process. This process is dependent on the profilin to actin ratio: when there is little profilin, branching proceeds as normal, while high amounts of profilin inhibit branching at later times. Incorporating formin further biases monomers towards linear networks, so that the branch density with a given concentration of formin and profilin is lower than with profilin or formin alone. This synergistic effect is what we set out to test using in vitro experiments, which forms the final Section **??** of this paper.

2   Simulation algorithm and assumptions

The simulation approach we employ uses the next reaction, or Gillespie, algorithm [10] to simulate a series of chemical reactions related to polymerization and branching. Such an approach, in which we assume the reactions are well-mixed, is relatively standard in the literature [9, 2], but in this work we add the simulation of branched actin networks. Similar to [20, 15], we explicitly simulate branched actin networks, since their geometry (the number of branches and length of each branch) determines the rate of monomer binding and the possibility of arp 2/3 complex binding to form another branch. Unlike in [20], however, we do not explicitly track individual actin monomers in

Parameter	Description	Value	Units
k_0^{d+}	Dimer formation rate	3.5×10^{-6}	$\mu M^{-1} \cdot s^{-1}$
k_0^{d-}	Dimer dissociation rate	0.041	s^{-1}
k_0^{t+}	Trimer formation rate	13×10^{-5}	$\mu M^{-1} \cdot s^{-1}$
k_0^{t-}	Trimer dissociation rate	22	s^{-1}
k_0^{b+}	Barbed end addition rate	11.6	$\mu M^{-1} \cdot s^{-1}$
k_0^{b-}	Barbed end dissociation rate	1.4	s^{-1}
k_0^{p+}	Pointed end addition rate	1.3	$\mu M^{-1} \cdot s^{-1}$
k_0^{p-}	Pointed end dissociation rate	0.8	s^{-1}

Table 1: Parameter values for filament nucleation and growth [27].

space, which allows us to reach longer time and lengthscales. Specifically, we do not introduce seed filaments to skip the lag phase of actin assembly [8], and are consequently able to explicitly simulate the actin nucleation reactions proposed in [27] to obtain a more accurate picture of how formin-based nucleation competes with spontaneous nucleation. This section gives a summary of the rules and rates we implement for the simulation of actin, formin, arp 2/3 complex, and profilin. Validation of each component of the algorithm can be found in Appendix A.

2.1 Spontaneous assembly

The process of actin polymerization can be separated into a nucleation step and elongation step. In the nucleation step, two actin monomers come together to form a dimer, which then must be joined by another monomer to form a trimer. A trimer has a barbed and pointed end, and monomers can associate at those ends with the same rate as longer filaments. The reactions in the system are therefore: dimer formation and breakup, trimer formation and breakup, and polymerization and depolymerization from the barbed/pointed end of each filament. Table 1 lists the parameters for each of these reactions, which come from the recent study [27].

2.2 Incorporating formins

To incorporate formin into our simulation, we make the following assumptions:

1. Formin can nucleate filaments by binding two actin monomers in the reaction $F + A + A \rightarrow$

Parameter	Description	Value	Units	Ref
$k_{\mathrm{for}}^{(n)}$	Filament nucleation by formin	2×10^{-4}	$\mu\mathrm{M}^{-2}{\cdot}\mathrm{s}^{-1}$	[21, Tab. S1]
k_{for}^{+}	Formin association to barbed ends	29.1	$\mu\mathrm{M}^{-1}{\cdot}\mathrm{s}^{-1}$	[29]
k_{for}^{-}	Formin dissociation from barbed ends	5×10^{-4}	s^{-1}	[13]
α_{for}	Growth for formin barbed ends (no profilin)	0.5		[13]

Table 2: Parameter values for formin. We choose an average of values reported in literature for the mammalian formin mDia1 and mDia2 (with the exception of nucleation which comes from budding yeast data Bni1p.)

FA_2, which is irreversible and has rate $k_{\mathrm{for}}^{(n)}$ [21, 36]. Following previous studies [21, 36], we do not allow formin nucleates to break apart.
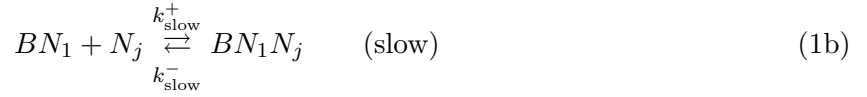
2. Fibers with formin at the barbed end add monomers with a modified rate $\alpha_{\mathrm{for}}k^{\mathrm{b+}}$ at the barbed end (the pointed end binding and unbinding rates are unchanged).

3. Formin can bind and unbind from existing filament barbed ends, with rates k_{for}^{+} and k_{for}^{-}, respectively.

We choose to model the mammalian formins mDia1 and mDia2, which are able to nucleate filaments from free actin monomers. For these formins, association of free monomers to barbed ends with bound formin takes place at roughly 50% the rate it does without formin [13]. The key rates are reported in Table 2, and Appendix A reports how we translate these rates into inputs to the simulation.

2.3 Arp 2/3 complex and branching

We now discuss our model of filament branching. Similar to previous work [20], we consider the binding of arp 2/3 complex to a linear filament, which results in the formation of a branch (the seventy degree angle is not relevant since our simulations do not resolve spatial dimensions [24]). We assume that arp 2/3 is always bound to its activator VCA. Previous work [4] has shown that the kinetics of actin monomers binding VCA-bound arp 2/3 complex are much faster than this complex (with or without a monomer attached) binding to an existing filament. Therefore, letting B be a VCA-bound arp 2/3 complex and N_j a filament of any size, the reaction proceeds in two

steps

$$B + N_1 \xleftrightarrow{K_{\text{fast}}} BN_1 \qquad \text{(fast)} \tag{1a}$$

$$BN_1 + N_j \underset{k_{\text{slow}}^-}{\overset{k_{\text{slow}}^+}{\rightleftarrows}} BN_1 N_j \qquad \text{(slow)} \tag{1b}$$

To simplify this, we assume the fast reaction is in equilibrium and coarse grain this process into a single reaction involving three reactants: (VCA-bound) arp 2/3 complex B, an actin monomer N_1, and an actin filament N_j,

$$B + N_1 + N_j \underset{k^{\text{br-}}}{\overset{k^{\text{br+}}}{\rightleftarrows}} BN_1 N_j. \tag{2}$$

The negative rate for this reaction is obtained from [4],

$$k^{\text{br-}} = k_{\text{slow}}^- = 3.4 \times 10^{-3}\,\text{s}^{-1},$$

while the positive rate can be obtained directly from the *in vitro* TIRF microscopy data in [30]. In that study, which uses budding yeast (for which branching is possible without bound VCA), the rate of branching is measured in units of $\mu\text{M}^{-1}\cdot\text{s}^{-1}$ per μm of mother filament. Because the branching occurs in a background of 1 μM monomeric actin, we can extrapolate the rate to the correct units by dividing by the background concentration to obtain

$$k^{\text{br+}} \approx 5 \times 10^{-3}\,\mu\text{M}^{-2} \cdot \text{s}^{-1}/(\mu\text{m of mother filament}).$$

This rate is an approximation, and represents a midpoint between the rate in the presence of VCA and the rate in its absence [30]. Because each monomer occupies an average of 2×10^{-3} μm, the rate we use is $10^{-5}\,\mu\text{M}^{-2} \cdot \text{s}^{-1}/(\text{monomer of mother filament})$.

To simplify the process of polymerization and depolymerization, we implement the following rules for branching:

1. A filament is eligible to form a branch when it has $N_{\text{mb}} = 4$ monomers or more. Once a branch forms, it forms on the fourth monomer or higher (the first three monomers cannot form branches).

2. The pointed end of the mother cannot unbind if a branch is sitting on the fourth monomer. This always leaves two monomers between the pointed end and the first branch.

3. The barbed end (of a mother or a branch) cannot unbind if another branch is attached to it.
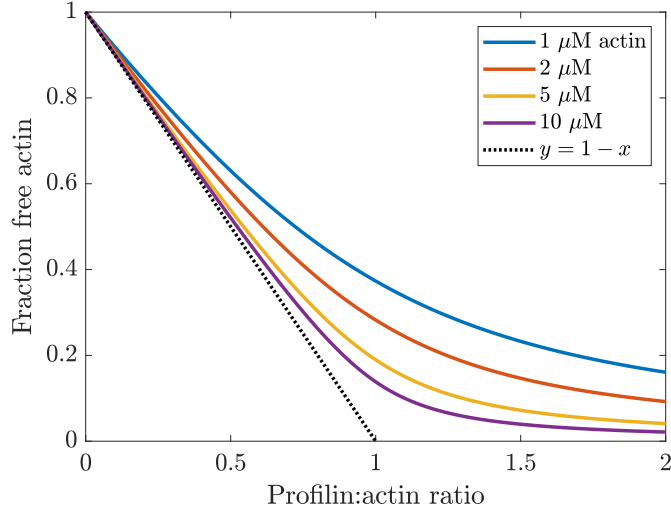
Figure 1: How the profilin:actin equilibrium affects the fraction of free actin. Here the x axis shows the ratio of profilin to actin, while the y axis shows the fraction of free monomers that result. Because of nonlinearities in the equilibrium, the curves are different for different actin concentrations. The dotted black curve shows the result if all the profilin binds to actin.

4. Branches can only unbind if they have length 1, in which case arp 2/3 also detaches from the filament (reverse of reaction (2)). "Barbed ends" alone cannot unbind if branches have length 1 (the only unbinding is through the reverse of reaction (2)).

This set of rules ensures simplicity in the construction and deconstruction of branched structures (in essence, the structure has to depolymerize in the order it was constructed, and cannot break into multiple branched structures). While these rules are certainly a simplification, our goal here is to study the number of branches per unit length, so whether one structure with 40 branches should in fact be two structures with 20 branches is of little consequence to us.

2.4 Profilin

Profilin is a protein which binds actin monomers in solution. The binding reaction has forward rate 45 $\mu\mathrm{M}^{-1}\cdot\mathrm{s}^{-1}$ and reverse rate 10 s^{-1} [23]. At typical profilin concentrations of order 1 μM, this reaction is much faster than the other reactions in the system, which means we can approximate it as in instantaneous equilibrium. Appendix A.1 discusses how we do this; in Fig. 1 we show the resulting fraction of free actin as a function of the profilin actin ratio. At low profilin concentrations, all of the profilin binds to actin, while at higher concentrations the equlibrium is more complex.

In our simulations, monomers bound to profilin cannot nucleate new filaments (dimers), regardless of whether or not they are assisted by formin [22]. Without formin, profilin-bound monomers bind barbed ends at a rate 80% of the free monomer value, while with formin the binding rate is 300% of the free monomer value (these represent average rates for mDia1 and mDia2 from [13]). Binding at the pointed end with profilin-bound monomers is small (10% of the free monomer value). Because profilin competes with VCA for binding actin monomers, and because VCA is (in most systems) required for arp 2/3 complex to bind an actin monomer and form a branch, we assume that branching with profilin-bound monomers is impossible.

3 Results

3.1 Linear filaments

3.1.1 Spontaneous assembly

We first consider the spontaneous assembly of actin filaments using the rates reported in [27]. As shown in Fig. 2A, the dynamics can be divided into the traditional three phases of actin polymerization: a "lag phase" for nucleation (which is longer for smaller concentrations), followed by a "growth phase" (in which free actin is incorporated into the existing fibers), terminated by an "equilibrium phase." At the end of the lag phase, the number of fibers per volume reaches a steady state, so that in the growth phase the decrease in free actin is driven exclusively by incorporation into existing fibers. After the growth phase is complete, the concentration of free actin remains constant at 0.17 μM, and the fibers must exchange monomers with other fibers to grow in length [12].

Similar to [2], we do not concern ourselves with the long-time "steady state" distribution of actin filament lengths, which can take days to reach [12, 9, 19], and instead focus on the length distributions on an intermediate timescale of a few hours, which corresponds to a typical timescale for *in vitro* experiments. Our results for the filament length distributions, which are shown in Fig. S4, match those of [2] for spontaneous nucleation of filaments: intermediate timescales show a quasi-stable length distribution which is skewed to the left and quite broad (c.f. [2, Fig. 2c]), and higher concentrations have lower mean filament lengths. More generally, conditions with a higher number of filaments have lower filament lengths beause of the limited actin pool.
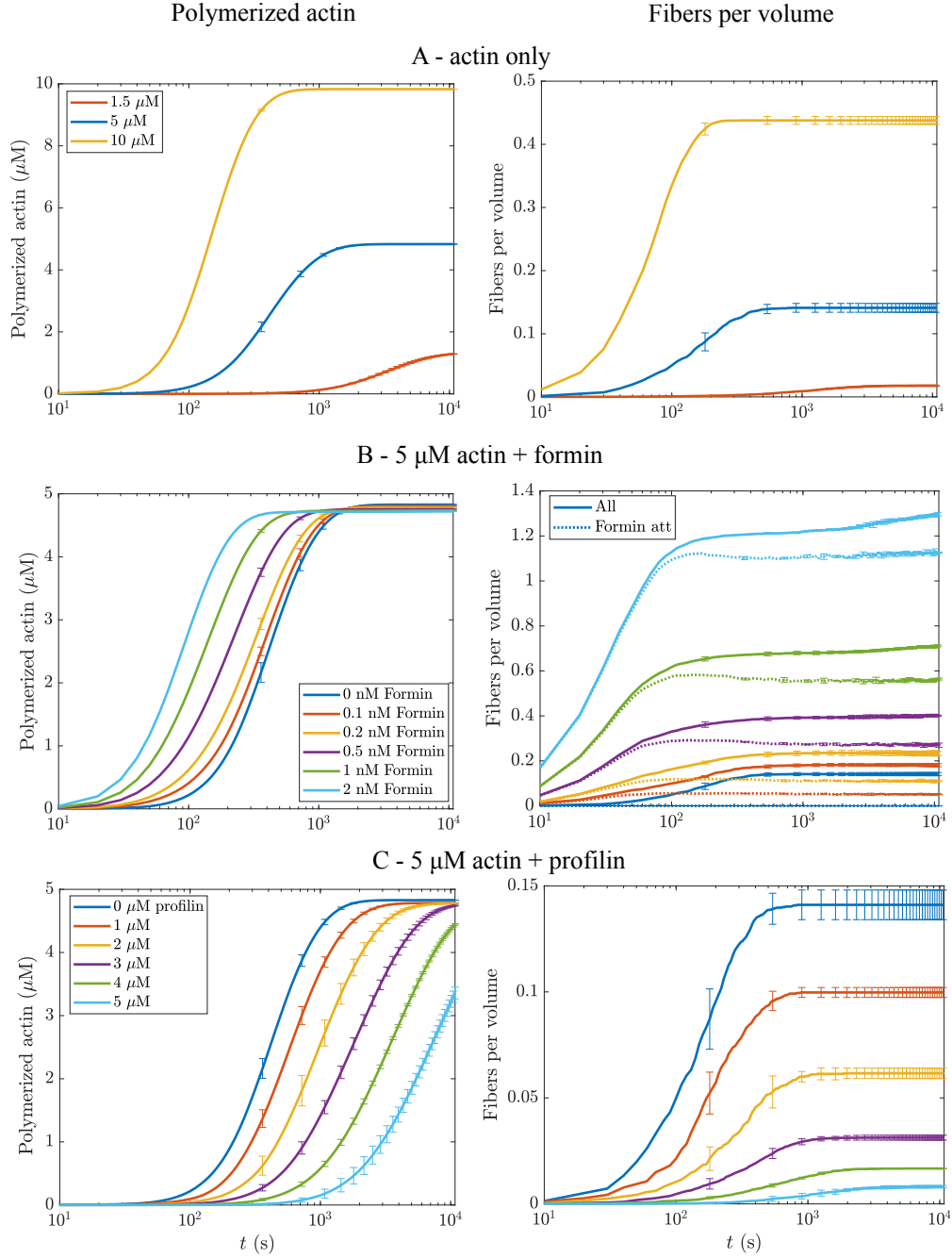
Figure 2: Stochastic simulations of polymerization dynamics at three different concentrations. In all cases, the concentration of polymerized actin is shown at left, and the number of fibers per μm^3 is shown at right. The blue curves (5 μM actin with no other proteins) are the same in all cases.

3.1.2 Incorporating formin

We now consider how adding formin affects the dynamics of actin polymerization at a fixed actin concentration of 5 μM (results for other concentrations are similar; in Fig. S7 we demonstrate this with 1.5 μM actin). Figure 2B shows the concentration of free monomers and fiber density (with and without bound formins) from simulations lasting three hours, in which we include formin at concentrations varying from 0 to 2 nM. In all cases, we see how formin aids the process of nucleation; at time shorter than 60 seconds, almost all of the filaments created are formin-bound, regardless of the formin concentration. As time goes on, the percentage of formin-bound filaments decreases in proportion to the amount of formin in the system, as spontaneous nucleation gives filaments without bound ends. The nucleation of additional filaments leads to a faster growth phase, since there are more barbed ends available to bind actin monomers. Thus, even though formin-bound barbed ends grow more slowly than free barbed ends, the additional barbed ends still lead to a faster growth phase. If we define the growth phase as the time it takes the free monomer concentration to go from 90% to 10%, we obtain a time of $252 - 30 \approx 200$ s with 2 nM formin, compared to $1080 - 144 \approx 1000$ s without formin. With 2 nM formin, there are ten times as many filaments, but each filament grows at half the speed, which gives a factor of five difference in the dynamics.

How do these dynamics affect the length distribution of fibers? As shown in Fig. S6, and as previously reported in [2], an increase in the formin concentration leads to the nucleation of more filaments at early times, which translates to a smaller mean and standard deviation in the number of monomers per filament. The slower speed of formin-filament growth leads to a bimodality in the distribution of filament lengths. The peak associated with formin-bound filaments tends to lose mass over time, in accordance with the theoretical expectation that the slower growing fibers (the formin-bound ones) will give up their actin over long times to the faster-growing (non formin-bound) ones [19].

3.1.3 Incorporating profilin

We next study how profilin affects polymerization without formin. Figure 2C compares the dynamics of polymerization of 5 μM actin with varying profilin concentrations in the range 0 to 5 μM. Low profilin concentrations do not show too much of a change from the spontaneous nucleation curves, since at 1 μM profilin concentration we only expect about 20% of the monomers to be bound to profilin. Increasing the profilin concentration has drastic effects; once we reach 5 μM profilin, the

growth phase is not complete by $t = 3$ hours. The slowdown in polymerization is driven by two factors: first, profilin has a reduced rate of binding for both pointed and barbed ends, which slows down the rate of polymerization. Second and more importantly, increases in profilin lead to less filaments being nucleated, which means there are less barbed ends available to bind monomers. The length distributions for each profilin concentration (Fig. S8) show another effect of having less filaments; each filament tends to be longer, and the distributions are more spread out. The reason for the latter is that there is no longer a big nucleation event that spawns many filaments. There are only a few filaments in the system, and the length of each filament is directly correlated with the time since it was nucleated.

3.1.4   Profilin and formin together

Figure 2 showed that formin and profilin have essentially opposite functions; formin speeds up overall polymerization by increasing nucleation, while profilin slows it down by inhibiting nucleation. The natural expectation is that putting formin and profilin together will rescue the original rate of polymerization. We examine this more closely in Fig. 3, where we consider two different actin concentrations (1.5 μM and 5 μM). For each actin concentration, we look at three different formin concentrations (0, 0.1, and 1 nM), and three different profilin:actin ratios (0:1, 0.5:1, and 1:1). There we observe a general trend: without formin, adding profilin slows down polymerization. Adding a small amount of formin (0.1 nM) to the reaction then rescues the original timescale of polymerization, in agreement with older bulk-actin polymerization curves in [14, Fig. 2] and [11, Fig. 6].

Because profilin-actin binds to formin-bound barbed ends faster than free actin, but also inhibits fiilament nucleation, there is an interesting trade-off between the lag phase and growth phase in the overall polymerization dynamics. At a fixed (nonzero) formin concentration, increasing the profilin conentration to an 0.5:1 ratio typically *speeds up* polymerization, since there is not enough profilin to completely block nucleation, and once filaments are nucleated they polymerize faster. Increasing to a 1:1 ratio then slows down polymerization because having almost all of the actin bound to profilin signficantly slows down the lag phase, so much so that the faster elongation phase can no longer catch up.
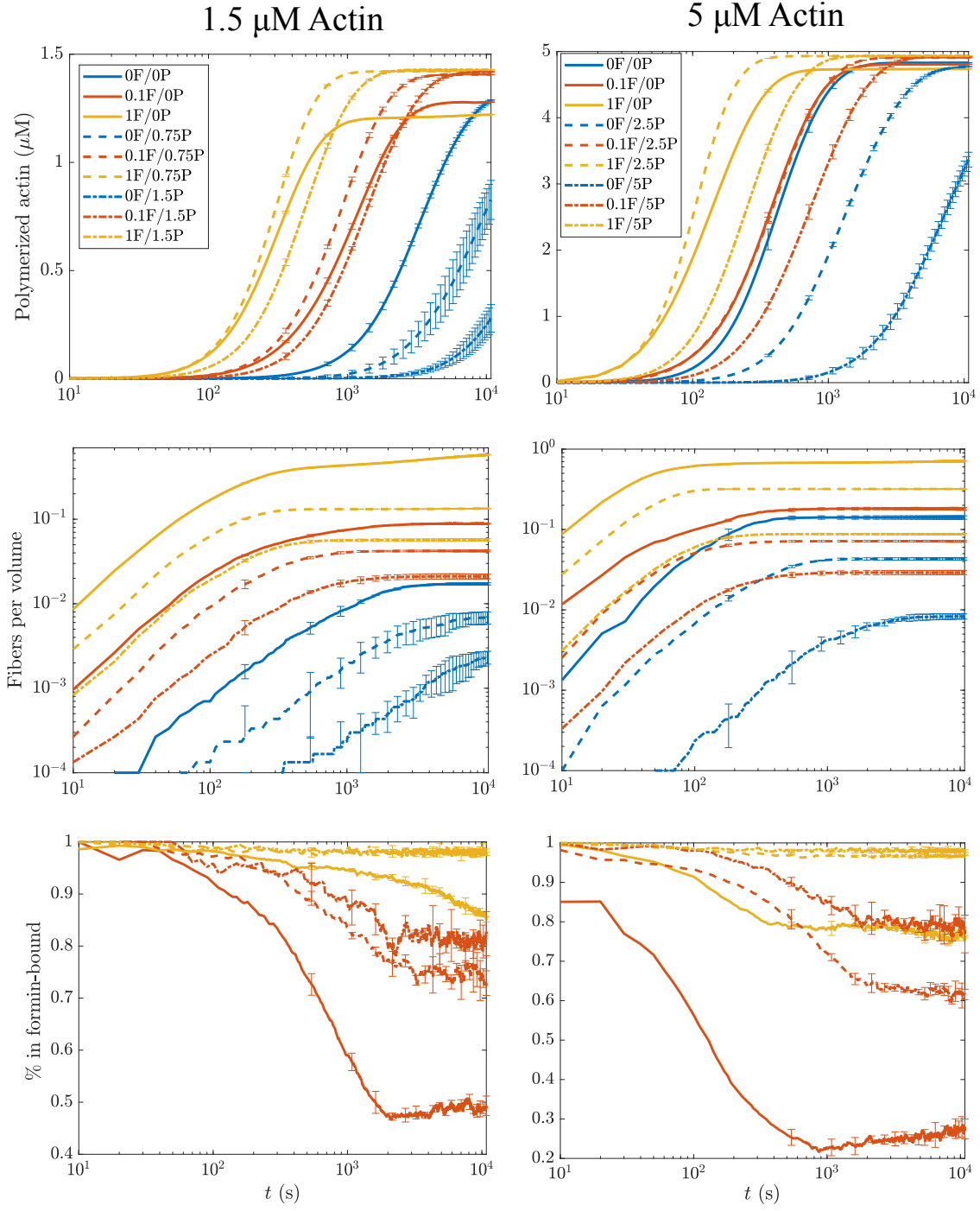
Figure 3: Dynamics of actin polymerization (at 5 μM) with formin and profilin. Left column shows 1.5 μM actin, right column shows 5 μM actin. In all cases, blue, red, and yellow curves show 0 nM formin, 0.1 nM formin, and 1 nM formin, respectively, while solid, dashed, and dashed-dotted curves show 0:0, 0.5:1, and 1:1 profilin:actin ratio, respectively. Top plots show the concentration of polymerized actin, middle plots show the number of filaments per μm^3, and bottom plots show the percentage of formin bound fibers.
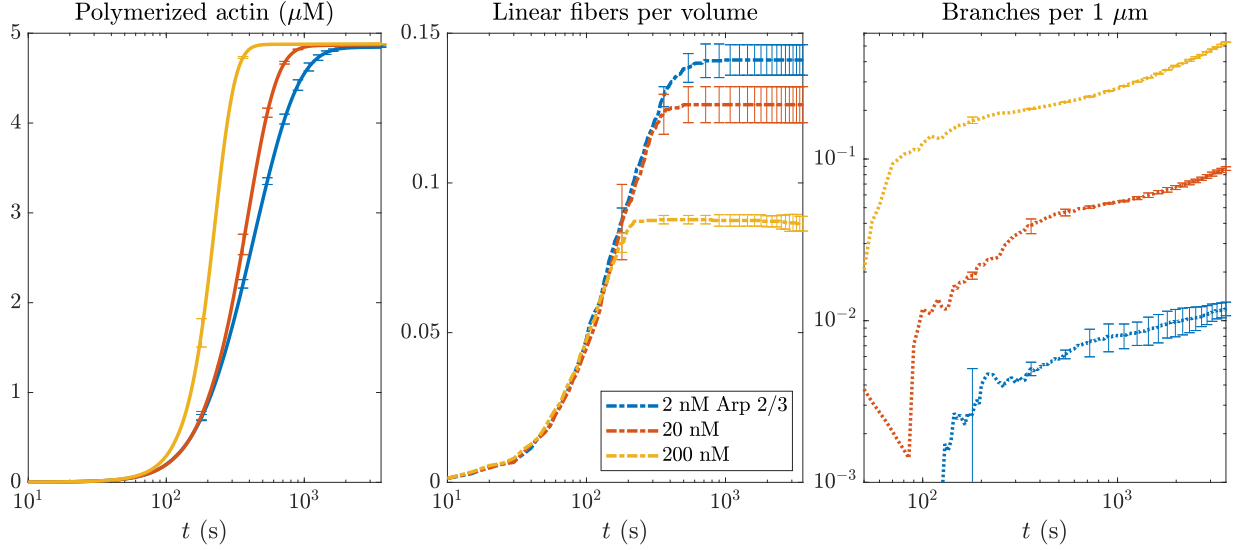
Figure 4: Course of polymerization and assembly with 5 μM actin concentration and various concentrations of arp 2/3 (2 nM in blue, 20 nM in red, and 200 nM in yellow). From left to right, these plots show the total amount of polymerized actin, the number of linear fibers (including mother filaments) per volume, and the number of branches per length.

3.2 Branched filaments

3.2.1 Branching with spontaneous nucleation

We begin by looking at the branching process with spontaneous nucleation of actin filaments only (no formins). We fix the actin concentration at 5 μM and vary the concentration of arp 2/3 across two orders of magnitude (2 nM, 20 nM, and 200 nM). The dynamics of polymerization and assembly are shown in Fig. 4, and the filament length distributions are shown in Fig. 5.

To understand these data, it is important to remember that actin filament polymerization with spontaneous nucleation proceeds in two phases: nucleation of filaments (slow), and then elongation (fast). Figure 4 shows that the speed of branching relative to these two timescales determines the behavior. In the case of 2 nM arp 2/3, significant branching does not appear until $t \approx 400$ s, at which time the nucleation phase is already complete. Thus in this case most of the actin sits in linear filaments, and there is a small number of branches (0.01) per μm. Increasing to 20 nM arp 2/3 and then 200 nM arp 2/3, the timescale of branching gets shorter, until it starts to compete with nucleation. At the highest arp 2/3 concentration, there are substantially fewer linear filaments, because branching on the filaments that do form takes up the available actin.

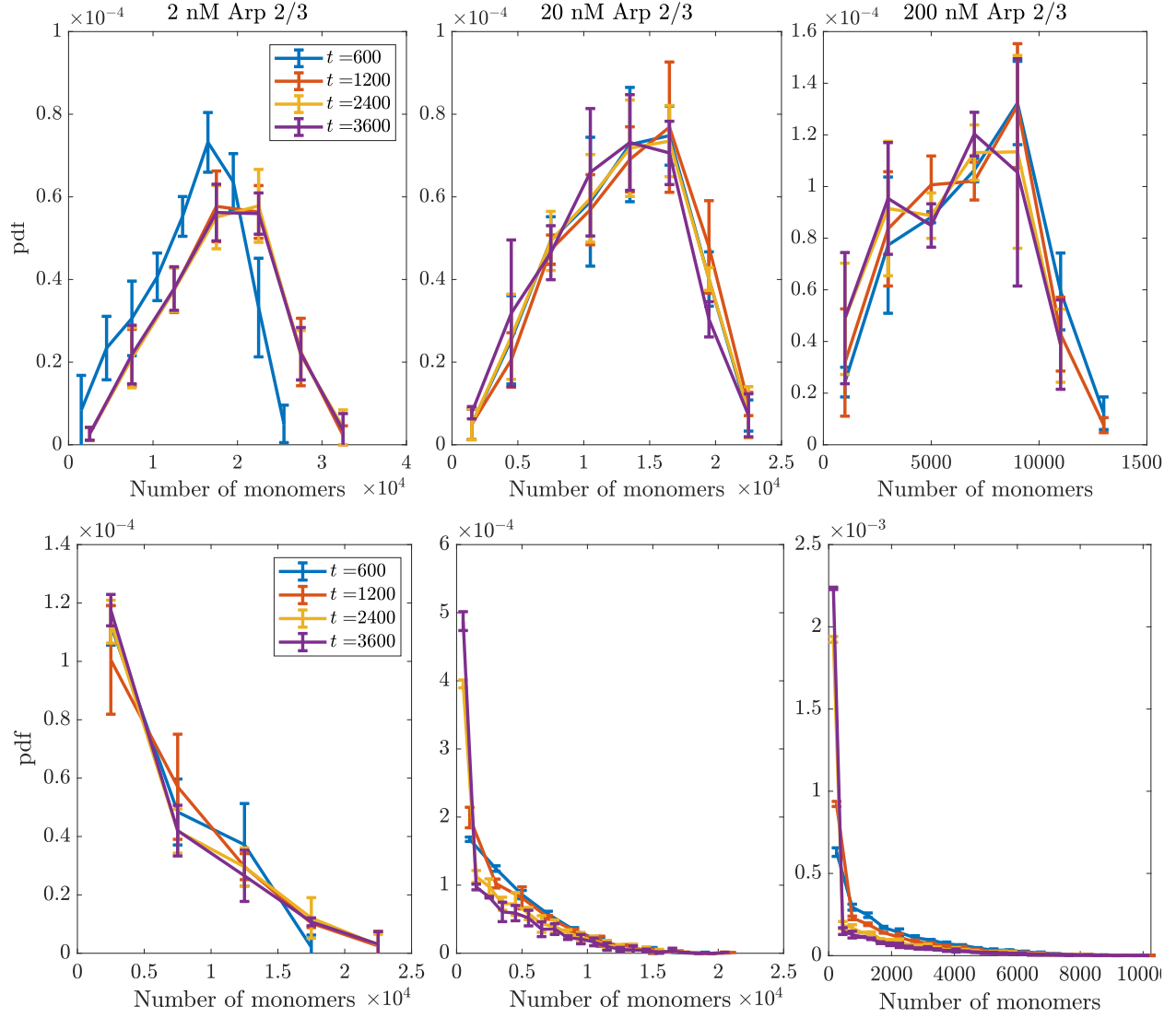Further understanding of the dynamics can be gained by looking at the length distributions in

Figure 5: The length distribution of filaments with 5 μM actin concentration and various concentrations of arp 2/3 (2 nM at left, 20 nM in the middle, and 200 nM at right). We separate the filaments into linear and mother filaments, and show their length distribution at the top, and branches, with their length distribution at the bottom.

Fig. 5, where we have made separate distributions for linear fibers (including mothers of branches) in the top set of plots, and branches in the bottom set. For 2 nM Arp 2/3 concentration, the length distributions look similar to the case without arp 2/3, where a quasi-steady state is achieved at roughly 1000 s that has a mean of 2×10^4 monomers. The branches sit in a rough steady state here, reflecting an equilibrium where monomers typically exchange between existing filaments. For 20 nM and 200 nM Arp 2/3 concentration, the quasi-steady state in the linear fibers occurs at an early time, and they do not elongate past 2×10^4 monomers. It is instead branches which form, in particular new branches, as the distribution of branch lengths becomes more and more concentrated on smaller branches over time. This is in line with our previous observation that branching is faster than elongation for these concentrations. The formation of new branches at later times demonstrates that there is an excess of arp 2/3 which looks for available monomers to form new branches.

3.2.2   Incorporating profilin

Because profilin competes with VCA for binding actin monomers, and because VCA is (in most systems) required for arp 2/3 complex to bind an actin monomer and form a branch, we assume that branching with profilin-bound monomers is impossible. With this assumption, Figure 6 shows the effect of adding profilin to a system of polymerizing actin and arp 2/3 complex.

Our observations for the branching process with profilin are similar to what we saw with linear filaments (Fig. S8). Increasing the profilin concentration slows down the nucleation and growth phase, since there are substantially less fibers nucleated. The branching process with profilin is significantly more interesting. When the profilin concentration is slow (1–2 μM), the branching rate initially ($t \leq 400$ s) is comparable to what it is without profilin. As more of the actin gets polymerized, the branching rate slows down substantially, because more of the actin is bound to profilin and so new branches cannot get nucleated. In systems without profilin, the branch density grows in the equilibrium phase, since free monomers can form new branches (especially when a lot of arp 2/3 is available). But with profilin, the branch rate is constant in the equilibrium phase; because the free actin concentration is low, almost all of it is bound to profilin, and no new branches can form.
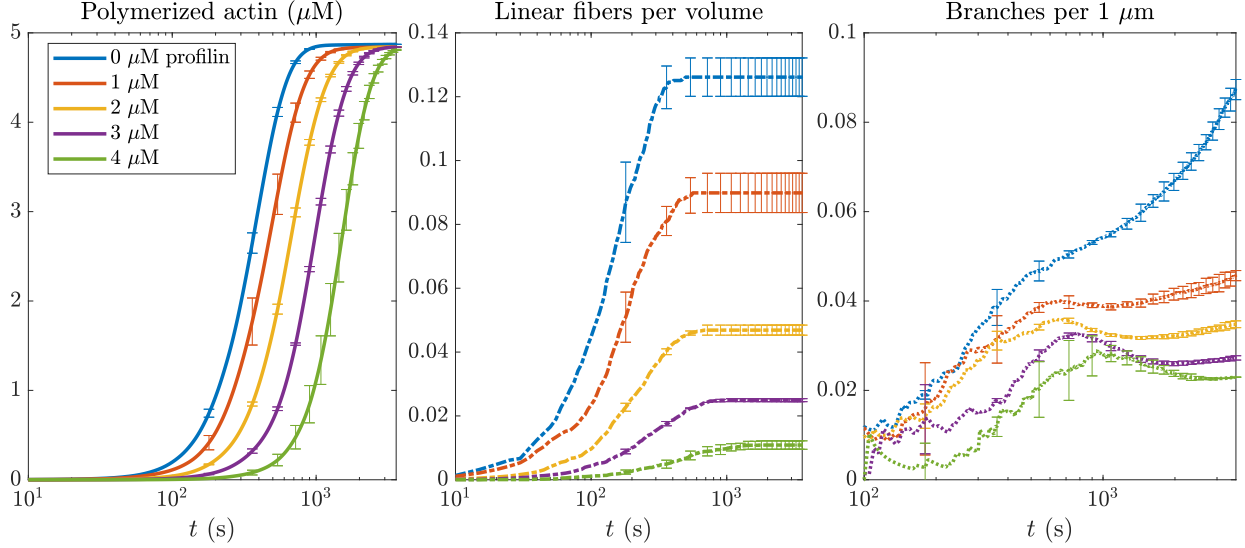
Figure 6: Course of polymerization and assembly with 5 μM actin concentration, and varying profilin concentration with 20 nM arp 2/3 complex. From left to right, these plots show the total amount of polymerized actin, the number of linear fibers (including mother filaments) per volume, and the number of branches per length. With profilin, the number of branches does not grow in the equilibrium phase.

3.2.3 Incorporating formins

We now incorporate formin into the branching dynamics. As in linear filaments, formin can bind to the barbed end of branched filaments and modify the growth rate there.

We first consider 5 μM actin and 1 nM formin with varying concentrations of arp 2/3, plotting the dynamics in Fig. 7. As we have already seen in Section 2.2, formin speeds up the nucleation phase and produces more filaments. In Fig. 7, we see that, regardless of the arp 2/3 concentration, there are initially about 0.6 fibers per μm^3 produced. What happens next depends on the concentration of arp 2/3 complex. When there is a small amount of arp 2/3, there are a small amount of branches that form, and the amount of linear filaments is roughly constant in time. At high arp 2/3 concentrations, a significant amount of branch formation occurs, so that the amount of linear filaments per volume drops. Because there are more branches at higher arp 2/3 concentrations, the percentage of barbed ends with a bound formin drops significantly. Finally, although there are more filaments in the case with formin, the total length of polymerized actin is the same, and so the number of branches per 1 μm does not change from the case without formin (c.f. Fig. 4).

Based on previous results, we now consider adding in profilin to a system with 1 nM formin and 20 nM arp 2/3. Without profilin, we saw that adding formin made little difference in the branch
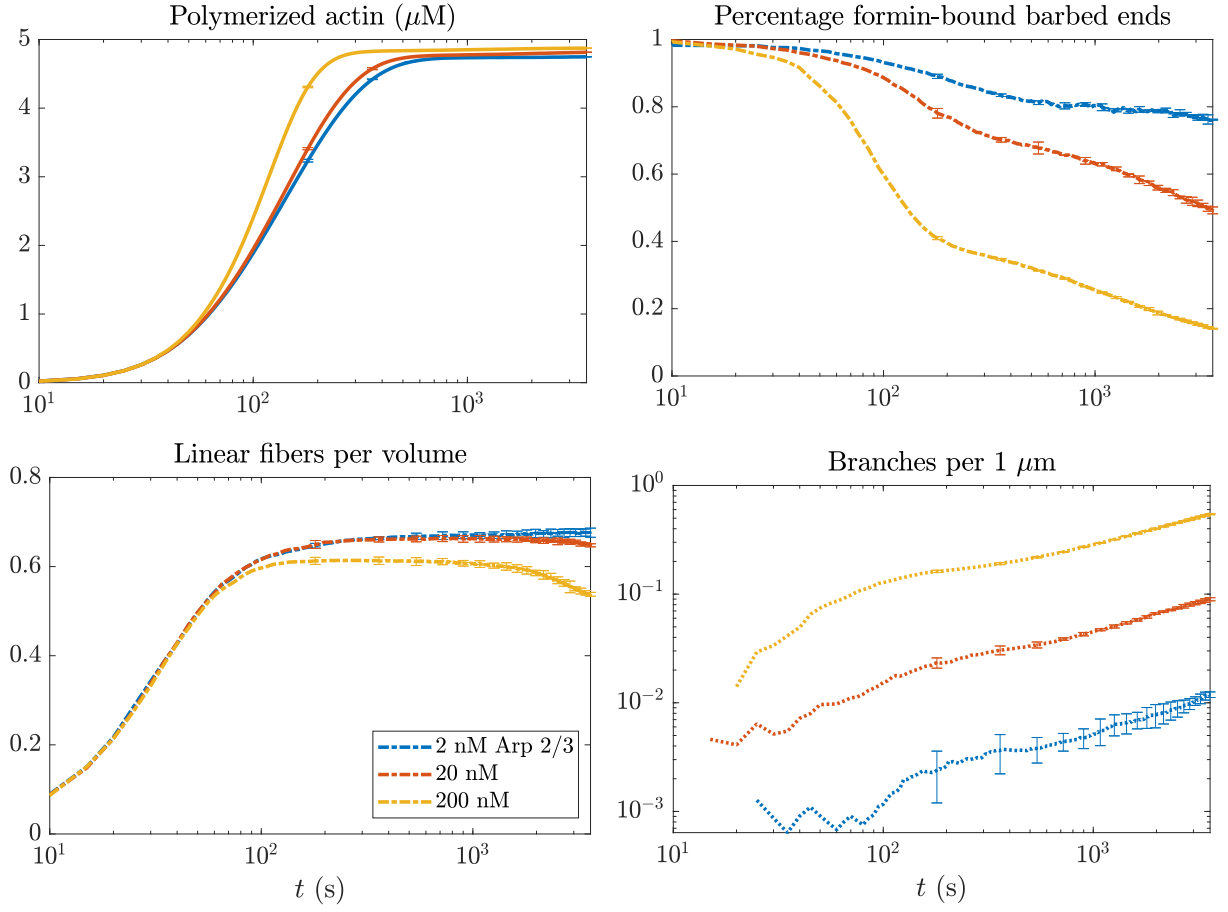
16

Figure 7: Course of polymerization and assembly with 5 μM actin concentration, 1 nM formin concentration, and three arp 2/3 concentrations. The top plots show the concentration of polymerized actin and the percentage of formin-bound barbed ends. The bottom plots show the dynamics of fiber and branch growth.

Figure 8: Course of polymerization and assembly with 5 μM actin concentration, 1 nM formin concentration, 20 nM arp 2/3 concentration, and varying profilin concentration. The top plots show the concentration of polymerized actin and the percentage of formin-bound barbed ends. The bottom plots show the dynamics of fiber and branch growth.

density; will this also be true when we add in profilin?

Figure 8 shows the results for a system that includes formin, arp, and profilin (everything). As we have seen previously, adding profilin reduces the number of fibers and number of branches. This means there are less barbed ends available, and so a higher fraction of the formin is bound to the barbed ends. As a result of profilin accelerating polymerization, the polymerization dynamics with profilin concentrations 1–3 μM are again faster than without profilin, which is the same conclusion we reached for linear fibers (see Fig. 3). But the faster dynamics have strong consequences for branching: for a fixed parameter set, the number of branches without formin (Fig. 6) is substantially *higher* than with formin. This is because the balance of rates has shifted; with profilin, polymerization of linear filaments is faster, and so more of the actin goes there than into the branches.

3.2.4 Summary of results

Our results on branching can be summarized as follows

- Branching occurs after the assembly of linear filaments. When the arp 2/3 concentration is high enough, the formation of new branches can compete with linear filaments, and there are less linear filaments at the end of the nucleation phase.

- Without profilin, new branches form in the equilibrium phase, and the number of branches constantly increases. With profilin, the number of branches remains constant in the equilibrium phase, because the free actin is all bound to profilin, and actin-profilin cannot form branches.

- With formin, there are more linear fibers per volume, but the branch density is unchanged from the case without formin (because the amount of polymerized actin is the same). This conclusion changes when we add profilin: because profilin-actin goes into formin-bound fibers at a faster rate, the number of branches drops relative to the case without formin. Thus,
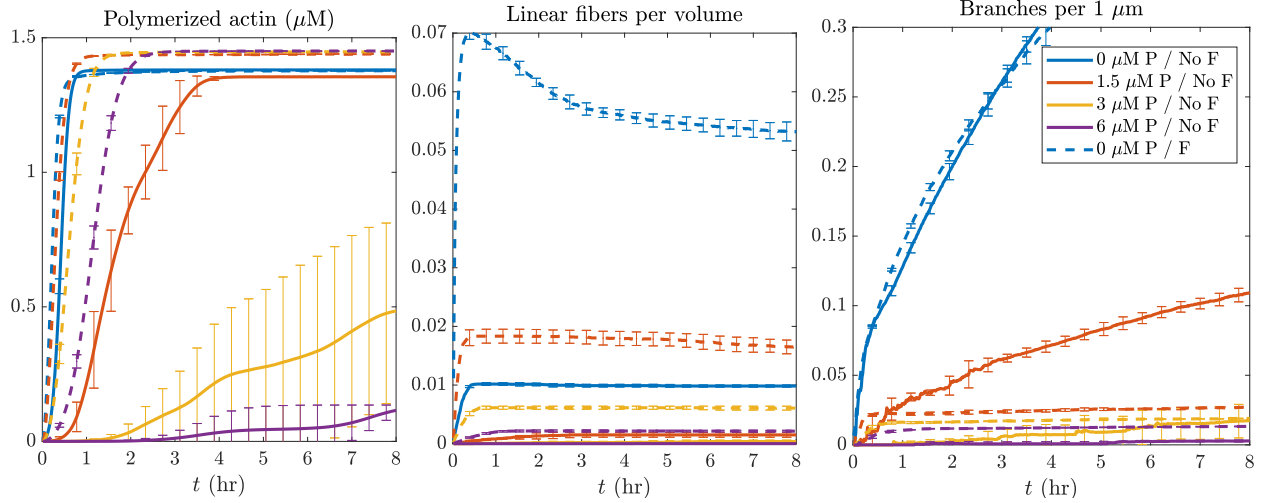
18

Figure 9: Polymerization and branching dynamics for more dilute systems. Conditions are 1.5 μM actin, 0.1 nM formin (for the dashed lines), and 40 nM arp 2/3. The profilin concentration varies as indicated in the legend.

if we wanted to use formin to reduce the branch frequency, we need to add profilin as well. (This would be a nice experiment to try.)

3.3 In vitro experiments

Typical TIRF experiments can only go up to actin concentrations of 1.5 μM. Figure 9 shows our experiments at this concentration. The same fundamental trends are observed, although a new regime emerges at very high profilin concentrations where there is no polymerization after 8 hours, and thus minimal branching. Thus, at zero profilin concentration the branch density is the same regardless of whether formin is around. Increasing to 1:1 profilin concentration gives lower branch densities with formin. Increasing to higher profilin concentration then gives higher branch densities (after 8 hrs) with formin, because the simulations without formin have not yet reached a steady state.

4 Conclusion

Our measurements for linear filaments revealed an interesting general property of the profilin/actin/formin interaction: if profilin inhibits spontaneous nucleation, while also speeding up polymerization in the presence of formin, a moderate amount of profilin can actually speed up the total speed of polymerization. Interestingly, measurements in mammalian cells placed the profilin:actin ratios
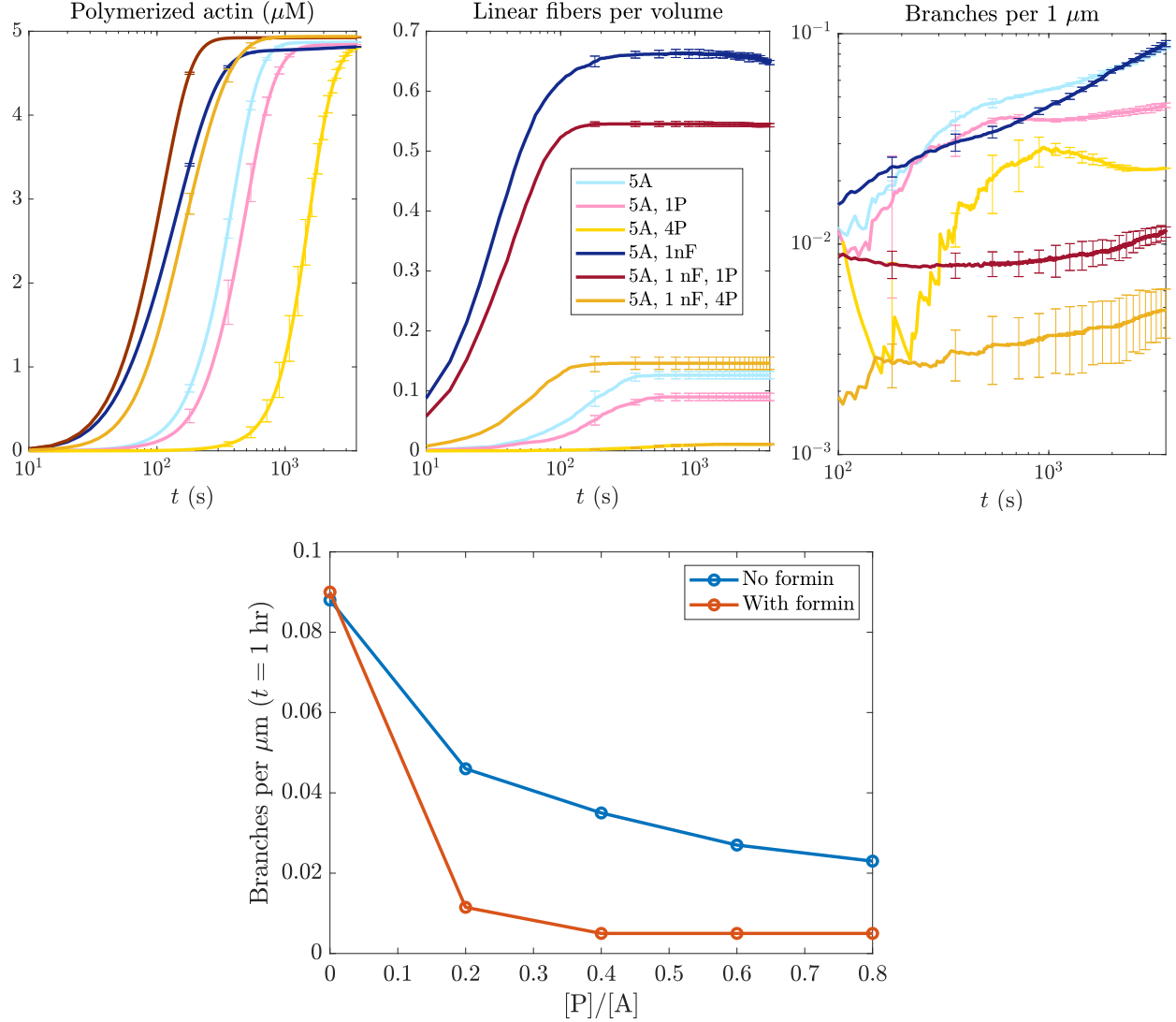
Figure 10: Summary of the role of formin and profilin for branched fiber growth (20 nM arp 2/3 in all cases). Top plots: We show the base 5 μM actin in light blue, with 1 μM profilin in pink and 4 μM profilin in yellow. The darker colors then show the same concentrations, but with 1 nM formin. Bottom plot: the number of branches per μm after one hour as a function of profilin concentration without (blue) and with (red) formin.

around 0.5:1, suggesting that *in vivo* dynamics operate in the regime where profilin speeds up, rather than slows down polymerization [**?**].

Appendix A   Algorithm and validation

This appendix contains the details of our algorithm and the validation. For validation, we use ODEs, and close the system by assuming a maximum of five monomers per fiber.

A.1   Stochastic simulation algorithm for linear filaments

To keep our algorithm general, let us suppose that we have P_M proteins which bind to monomers in solution, and are kicked off of the monomers once they bind to fibers. We also assume that there are P_B proteins which bind barbed ends of actin filaments. Letting M be the total number of free actin monomers, and $M^{(0)}$ the amount of free actin monomers attached to no protein. The equilibrium reactions .

$$M^{(0)} + P^{(i)} \overset{\kappa^{(i)}}{\longleftrightarrow} M^{(i)} \tag{S2a}$$

$$M^{(i)} = \kappa^{(i)} M^{(0)} \left(P^{(i)} - M^{(i)} \right) \to M^{(i)} = \frac{\kappa^{(i)} M^{(0)} P^{(i)}}{1 + \kappa^{(i)} M^{(0)}} \tag{S2b}$$

dictate the number of monomers attached to protein $i \geq 1$. In the case when there is only one monomer, the equation

$$M^{(0)} + M^{(1)} = M^{(0)} + \frac{\kappa^{(1)} M^{(0)} P^{(1)}}{1 + \kappa^{(1)} M^{(0)}} = M \tag{S2c}$$

can be solved to obtain a closed-form solution for the amount of free monomers

$$M^{(0)} = \frac{1}{2\kappa^{(1)}} \left(- \left(1 + \kappa^{(1)} \left(P^{(1)} - M \right) \right) + \sqrt{ \left(1 + \kappa^{(1)} \left(P^{(1)} - M \right) \right)^2 + 4\kappa^{(1)} M } \right). \tag{S2d}$$

Thus, prior to calculating any reaction rates, the first step of our reaction algorithm is to compute the number of monomers attached to each protein using (S2).

For our reactions, we let $k_{ij}^{\mathrm{d+}}$ be the rate of dimer formation for monomers bound to protein i (starting from 0, to include no bound protein), and barbed end bound to protein j (starting from 0, again to include no protein). Likewise, $k_{ij}^{\mathrm{t+}}$ is the rate of trimer formation, and $k_{ij}^{\mathrm{f+}}$ is the rate of addition to fibers (length 3 or more). The rate of addition to fibers is broken into $k_{ij}^{\mathrm{f+}} = k_i^{\mathrm{p+}} + k_{ij}^{\mathrm{b+}}$, since the pointed end rate is assumed to depend only on the protein bound to the monomer, while the barbed end addition rate depends on both bound proteins. The rates of unbinding $k_j^{\mathrm{f-}} = k^{\mathrm{p-}} + k_j^{\mathrm{b-}}$

21

are a function of the barbed-bound protein only. Finally, we let k_j^{on} and k_j^{off} be the rates of binding and unbinding of the barbed end proteins.

Given this notation, the next reaction method proceeds as follows: at the beginning of each step, we compute the total number of monomers bound to each protein via (S2). Then, we sample a time for each of the following reactions to occur:

1. *Spontaneous dimer formation.* For all i and $j = 0$, dimer formation occurs with rate $(k_{i0}^{\text{d+}}/V)M^{(i)}M^{(i)}$.

2. *Barbed-bound-protein-induced nucleation.* For all i and $j > 0$, dimer formation occurs with rate $(k_{ij}^{\text{d+}}/V^2)M^{(i)}M^{(i)}B^{(j)}$.

3. *Dimer break-up.* For all j, each individual dimer breaks up with rate $k_j^{\text{d-}}$.

4. *Trimer formation.* For all i and j, each individual dimer becomes a trimer with rate $(k_{ij}^{\text{t+}}/V)M^{(i)}$.

5. *Trimer breakup.* For all j, each individual trimer breaks up with rate $k_j^{\text{t-}}$.

6. *Fiber growth.* For each individual fiber of length 3 or more, fiber growth occurs with rate $(k^{\text{f+}}/V)M^{(i)}$, where $k^{\text{f+}} = k_i^{\text{p+}} + k_{ij}^{\text{b+}}$.

7. *Fiber shrinkage.* For each individual fiber of length 4 or more with barbed bound protein j, removal of monomers occurs at the barbed end with rate $k_j^{\text{b-}}$ and at the pointed end with rate $k^{\text{p-}}$ (this is actually two reactions).

8. *Barbed protein binding.* Barbed protein j binds to each fiber of length 2 or more with rate $k_j^{\text{on}}B^{(j)}$.

9. *Barbed protein unbinding.* Barbed protein j unbinds from each fiber that it is attached to with rate k_j^{off}.

We use an exact Gillespie simulation algorithm [10] to simulate these reactions. If a reaction has rate r_i, we sample a time for it to occur according to an exponential distribution, $\Delta t_i = -\log(u)/r_i$, where $u \in (0, 1]$. The reaction chosen is then the one that occurs soonest. Once a reaction is chosen, we increment time by this minimum amount and process the reation by changing the state of the system to reflect its outcome (e.g., unbinding from the barbed end removes one monomer from a filament and adds it to the free monomer count). We then repeat this entire process (including the

calculation of bound monomers in (S2)) until the time step is complete. Because this is an exact simulation algorithm, the time step Δt is arbitrary and is not a restriction on accuracy.

To efficiently implement these reactions, we take an approach where we track a number of fiber nucleates, which we denote as $B_m^{(j)}$ for $m = 2, 3$. Once fibers reach a size of four, we create an object in space to track each of them individually.

A.1.1 Algorithm validation

We validate our stochastic simulation algorithm by comparing to ODEs. To facilitate this, we must cap the length of fibers at a maximum size M, which we set to $M = 5$. To formulate the ODEs, we begin by defining the rate at which monomers become dimers with the barbed end bound with protein j. Given the rates and reactions defined in Section A.1, this rate is given by

$$R_2^{(0)} = \sum_{i=0}^{P_M} \left(k_{i0}^{\mathrm{d+}} M^{(i)} M^{(i)} \right) - k_0^{\mathrm{d-}} B_2^{(0)} \qquad R_2^{(j>0)} = \sum_{i=0}^{P_M} \left(k_{ij}^{\mathrm{d+}} M^{(i)} M^{(i)} B^{(j)} \right) - k_j^{\mathrm{d-}} B_2^{(j)} \qquad \text{(S3a)}$$

The rate at which dimers become trimers is given by

$$R_3^{(j)} = \sum_{i=0}^{P_M} \left(k_{ij}^{\mathrm{t+}} M^{(i)} B_2^{(j)} \right) - k_j^{\mathrm{t-}} B_3^{(j)}, \qquad \text{(S3b)}$$

and the rates at which fibers of larger sizes are formed are

$$R_m^{(j)} = \sum_{i=0}^{P_M} \left(k_{ij}^{\mathrm{f+}} M^{(i)} B_{m-1}^{(j)} \right) - k^{\mathrm{f-}} B_m^{(j)}, \qquad 4 \leq m \leq M. \qquad \text{(S3c)}$$

Finally, the rate at which barbed binding proteins bind and unbind from the bound end of a fiber of size m is

$$S_m^{(j)} = k_j^{\mathrm{on}} B^{(j)} B_m^{(0)} - k_j^{\mathrm{off}} B_m^{(j)}. \qquad \text{(S3d)}$$

With these intermediates defined, the ODEs that govern the dynamics are

$$\frac{dM}{dt} = \sum_{j=0}^{P_B} \left(-2R_2^{(j)} - \sum_{m=3}^{M} R_m^{(j)} \right) \qquad \text{(S3e)}$$

$$\frac{dB^{(j)}}{dt} = -R_2^{(j)} - S_m^{(j)} \qquad \text{(S3f)}$$

$$\frac{dB_m^{(j)}}{dt} = \begin{cases} R_m^{(j)} - R_{m+1}^{(j)} - S_m^{(j)} & j = 0, \quad 2 \leq m < M \\ R_m^{(j)} - R_{m+1}^{(j)} + S_m^{(j)} & j > 0, \quad 2 \leq m < M \\ R_m^{(j)} - S_m^{(j)} & j = 0, \quad m = M \\ R_m^{(j)} + S_m^{(j)} & j > 0, \quad m = M \end{cases} \qquad \text{(S3g)}$$
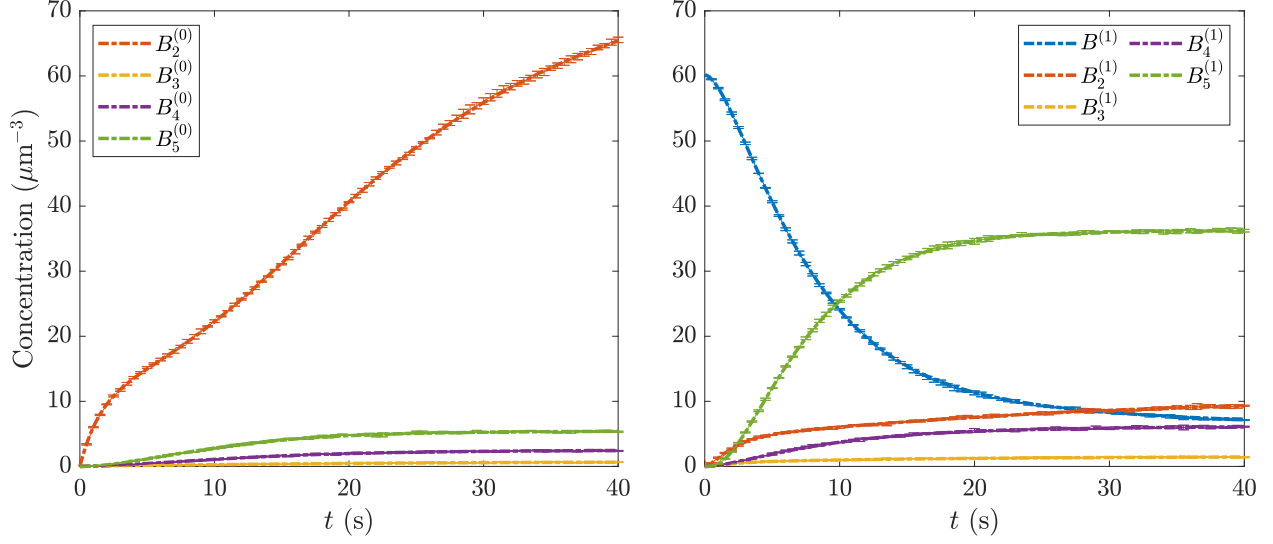
23

Figure S1: Validating the stochastic simulation algorithm with one monomer-binding and one barbed-binding protein. We consider an actin concentration of 2 μM in a box of size 3 μm on each side, and the rates given in (S4). The dashed-dotted lines show the concentration (in units μm^{-3}) of each particular species ($B_m^{(j)}$ denotes a polymer of size m with barbed protein j bound to it) predicted by the ODEs (S3). The solid lines with error bars show the output from the stochastic simulations. These data points show the mean over 3 sets of 10 simulations, with the error bars the standard error in the mean.

We validate our code by comparing the ODEs to stochastic simulations with the following rates

$$k_{ij}^{\mathrm{d+}} = 3.5 \times 10^{-3}\,\mu\mathrm{M}^{-1}\cdot\mathrm{s}^{-1} \begin{pmatrix} 1 & 0.57\,\mu\mathrm{M}^{-1} \\ 1.7 & 0.29\,\mu\mathrm{M}^{-1} \end{pmatrix} \qquad k_{ij}^{\mathrm{t+}} = 0.13\,\mu\mathrm{M}^{-1}\cdot\mathrm{s}^{-1} \begin{pmatrix} 1 & 10 \\ 0.4 & 2 \end{pmatrix}$$

$$k_{ij}^{\mathrm{b+}} = 1.6\,\mu\mathrm{M}^{-1}\cdot\mathrm{s}^{-1} \begin{pmatrix} 1 & 2 \\ 0.2 & 2.5 \end{pmatrix} \qquad k_i^{\mathrm{p+}} = 1.3\,\mu\mathrm{M}^{-1}\cdot\mathrm{s}^{-1} \begin{pmatrix} 1 & 0.25 \end{pmatrix} \qquad (\mathrm{S4})$$

$$\kappa_1 = 5\,\mu\mathrm{M} \qquad P^{(1)} = 0.05\,\mu\mathrm{M} \qquad B^{(1)}(t=0) = 0.1\,\mu\mathrm{M} \qquad k_1^{\mathrm{on}} = 5\,\mu\mathrm{M}^{-1}\cdot\mathrm{s}^{-1} \qquad k_1^{\mathrm{off}} = 8.1 \times 10^{-2}\,\mathrm{s}^{-1}$$

$$k_j^{\mathrm{d-}} = 0.041\,\mathrm{s}^{-1} \begin{pmatrix} 1 & 0.2 \end{pmatrix} \qquad k_j^{\mathrm{t-}} = 22\,\mathrm{s}^{-1} \begin{pmatrix} 1 & 0.4 \end{pmatrix} \qquad k^{\mathrm{p-}} = 0.8\,\mathrm{s}^{-1} \qquad k^{\mathrm{b-}} = 1.4\,\mathrm{s}^{-1} \begin{pmatrix} 1 & 0.1 \end{pmatrix}$$

Figure S1 shows that the solution of the ODEs (dashed-dotted lines) matches the output from stochastic simulations, thus validating all parts of our algorithm up to the branching of filaments.

24

A.1.2 Rates for formin and profilin

In the language of our simulation platform, the rates with formin and profilin are

$$k_1^{\text{on}} = 29.1 \, \mu\text{M}^{-1} \cdot \text{s}^{-1} \qquad k_1^{\text{off}} = 5 \times 10^{-4} \, \text{s}^{-1}$$

$$k_j^{\text{d-}} = k_0^{\text{d-}} \begin{pmatrix} 1 & 0 \end{pmatrix} \qquad k_j^{\text{t-}} = k_0^{\text{t-}} \begin{pmatrix} 1 & 0 \end{pmatrix} \qquad k^{\text{b-}} = k_0^{\text{b-}} \begin{pmatrix} 1 & 1 \end{pmatrix},$$

$$k_{ij}^{\text{d+}} = k_0^{\text{d+}} \begin{pmatrix} 1 & 0.057 \, \text{nM}^{-1} \\ 0 & 0 \, \text{nM}^{-1} \end{pmatrix} \qquad k_{ij}^{\text{t+}} = k_0^{\text{t+}} \begin{pmatrix} 1 & 5.5 \times 10^4 \\ 0 & 2.8 \times 10^5 \end{pmatrix}$$

$$k_{ij}^{\text{b+}} = k_0^{\text{b+}} \begin{pmatrix} 1 & 0.5 \\ 0.8 & 3 \end{pmatrix} \qquad k_i^{\text{p+}} = k_0^{\text{p+}} \begin{pmatrix} 1 & 0.1 \end{pmatrix}.$$

where the base rates are given in Table 1. Note the large rate for the trimers; we assume that formin-bound dimers become trimers with rate $\alpha_{\text{for}} k_0^{\text{b+}} + k_0^{\text{p+}}$, which is divided by $k_0^{\text{t+}}$ to obtain the proportion (α_{for} is 0.5 without profilin and 3 with profilin). We assume that formin bound dimers and trimers do not depolymerize.

A.2 Branched filaments

Given the set of rules formulated in Section 3.2, we can now formulate the reactions involving arp 2/3 complex. Letting D be the number of free arp 2/3 complexes, the reactions are

1. *Branch formation.* Each fiber (or branch) of length 4 or more can form a branch with rate $r = \left(k_i^{\text{br+}}/V^2 \right) D M^{(i)} m$, where m is the number of monomers on the fiber. If this reaction is selected, we form a new branch with one monomer at a 70 degree angle from the mother filament (chosen at random from the branches once a particular structure is selected).

2. *Branch unbinding.* Branches of length one can come off the mother filament with rate $k^{\text{br-}}$.

3. *Branch polymerization.* For each i, branches can polymerize from their barbed ends only with rate $\left(k_{ij}^{\text{b+}}/V \right) M^{(i)}$.

4. *Branch depolymerization.* Branches can depolymerize from their barbed ends with rate $k^{\text{b-}}$, as long as the geometry permits it (see rules above).

5. *Barbed protein binding and unbinding.* These are the same reactions as for linear fibers.

Because of the spatial complexity of branched networks, it is difficult to validate depolymerization using ODEs, as it becomes complicated to work out the probability that an unbinding event, if

selected, will actually be successful. Because of this, we divide our validation work into two steps: all events *other than* depolymerization, and depolymerization alone. The first case allows us to work with ODEs, as we have done previously, while the second requires us to synthesize a specific structure and look at its depolymerization.

A.2.1 ODE-based validation (excludes depolymerization)

In the presence of branching, additional terms are required for the ODEs. We let D be the number of arp 2/3 complexes, and $D_m^{(j)}$ be a branch of length m with barbed-bound protein j. If $k^{\mathrm{br+}}$ is a rate of branching in units of concentration$^{-2} \times$ s^{-1} per monomer of mother filament, the total rate of branch formation is

$$R_b = D \left(\sum_{i=0}^{P_M} k_i^{\mathrm{br+}} M^{(i)} \right) \left(\sum_{j=0}^{P_B} \sum_{m=4}^{M} m D_m^{(j)} \right) - k^{\mathrm{br-}} \sum_j D_1^{(j)}. \tag{S5a}$$

In addition to forming and being removed, branches exchange barbed proteins with rates given by (S3d), and the flux between branches of size m and size $m-1$ is given by

$$C_m^{(j)} = \sum_{i=0}^{P_M} \left(k_{ij}^{\mathrm{b+}} M^{(i)} D_{m-1}^{(j)} \right) - k^{\mathrm{b-}} D_m^{(j)}, \qquad 2 \leq m \leq M, \tag{S5b}$$

which is (S3c) with polymerization from the barbed end only. It is straightforward to combine these rates into equations for D and $D_m^{(j)}$. The only complication becomes if a depolymerization event is successful. For branching, we combine the rates in (S4) with the additional branching rates,

$$k_i^{\mathrm{br+}} = 10^{-2} \, \mu\mathrm{M}^{-2} \cdot \mathrm{s}^{-1} \begin{pmatrix} 1 & 1.3 \end{pmatrix} \qquad k^{\mathrm{br-}} = 0.5 \, \mathrm{s}^{-1} D(t=0) = 0.1 \, \mu\mathrm{M} \tag{S6}$$

to validate our code *without* depolymerization of barbed and pointed ends (i.e., $k^{\mathrm{b-}} = k^{\mathrm{p-}} = 0$). Figure S2 shows that the trajectories we obtain from simulations (mean over 10 trajectories repeated 3 times for error bars) match those predicted by the ODEs.

A.2.2 Structure-based validation for depolymerization

Let us consider the structure shown in Fig. S3. It is composed of a mother filament with 4 monomers, and then three branches with 6, 8, and 10 monomers. Because each branch is attached to the previous one, our rules state that this filament can only depolymerize linearly. The average time to depolymerize the branches (remove all the blue monomers) should be $21/k^{\mathrm{b-}} + 3/k^{\mathrm{br-}}$, since there are 21 monomers not attached to arp 2/3 and 3 monomers attached to arp 2/3. If
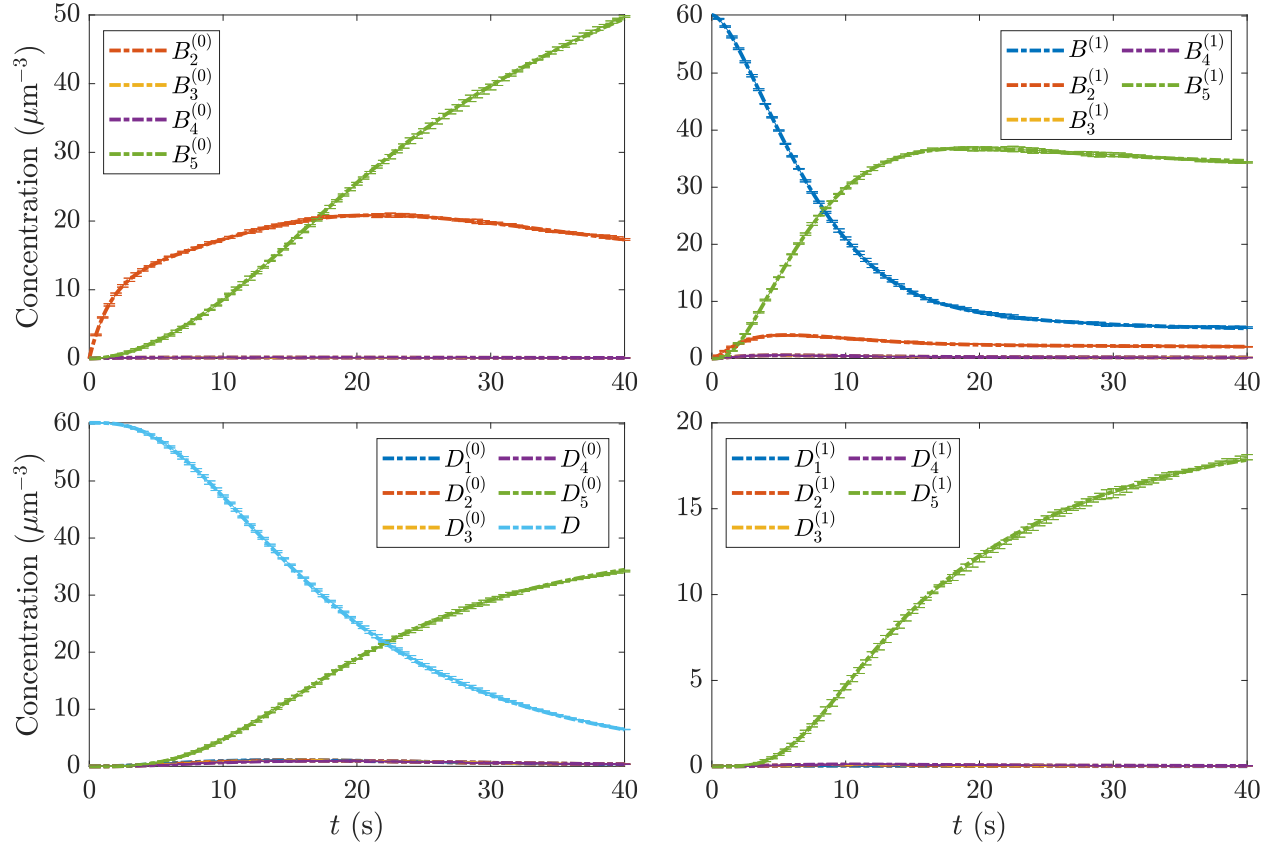
Figure S2: Validating the stochastic simulation algorithm with formins and arp 2/3 complex, where we only allow growth of fibers. We compare our stochastic simulations to ODEs (based on (S3) and (S5) with rates given in (S4) and (S6)).
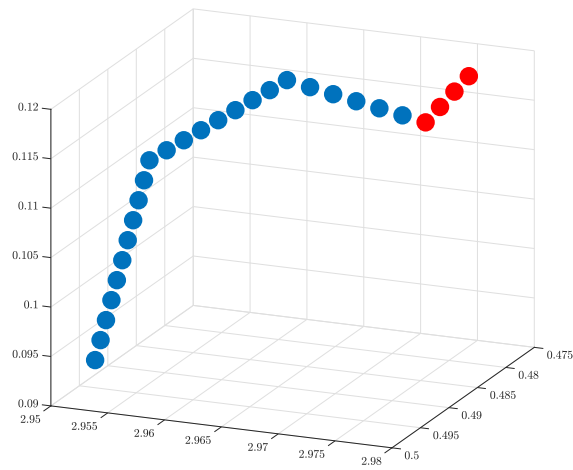

Figure S3: The branched geometry for the depolymerization test. Red points show the mother filament, blue the branches.
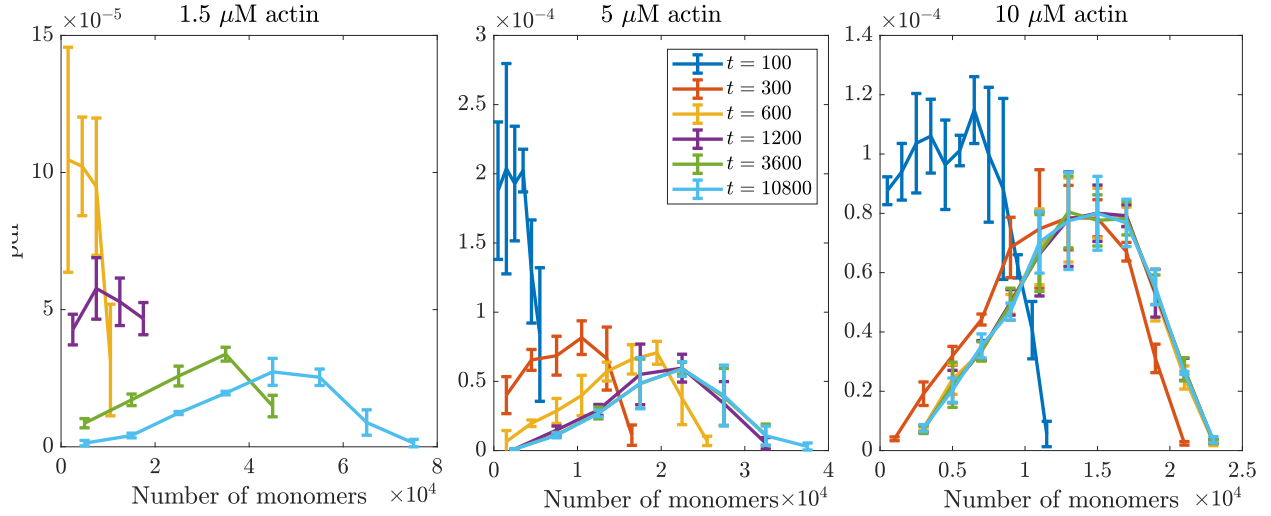
Figure S4: Stochastic simulations of polymerization dynamics at three different concentrations. The distribution of fiber sizes (in terms of the number of monomers) at three different time points for each concentration.

$k^{\text{b-}} = 1.4/\text{s}$ and $k^{\text{br-}} = 0.5/\text{s}$, this comes out to $6 + 15 = 21$ s. To verify that our code reproduces this depolymerization time, we perform a set of 1000 simulations with depolymerization only and record the time it takes for the filament to collapse down to the mother filament. This time is 20.9 ± 0.2 (error bar generated by repeating 20 times), which validates our implementation.

In the case when the mother filament has length 8 instead of 4, the time does not change significantly (21.1 ± 0.5), since the three monomers at the pointed end can unbind rapidly ($k^{\text{p-}} = 0.8/\text{s}$). The time does change significantly when we put all the branches onto the same barbed end of the mother filament. In this case, all of the branches can depolymerize simultaneously, and the measured time for depolymerization is 9.9 ± 0.1 s, which is slightly longer than the theoretical time for the longest branch ($9/k^{\text{b-}} + 1/k^{\text{br-}} = 8.4$ s) to unbind, in accordance with the theoretical expectation that the expected value maximum is longer than the expected value of the longest event.

Appendix B   Results on linear filaments

References

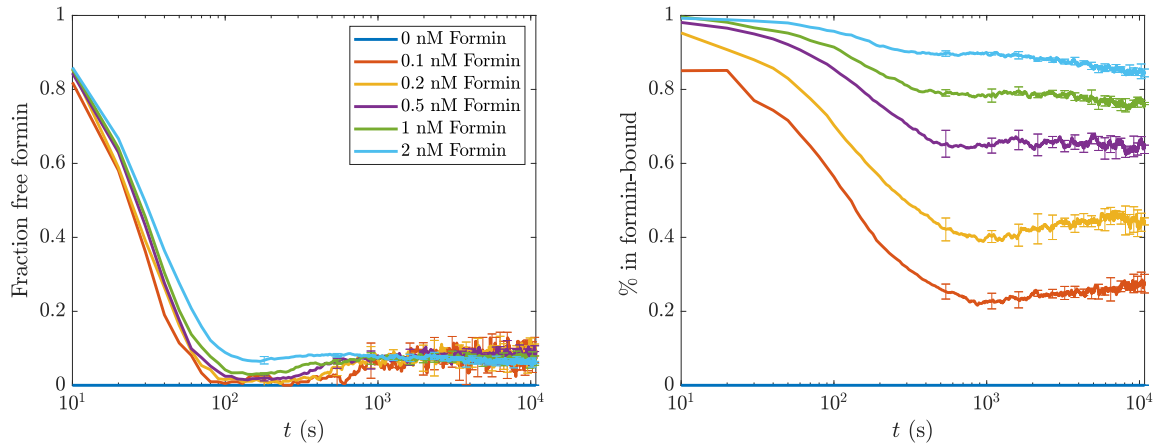[1] Bruce Alberts. *Molecular biology of the cell*. WW Norton & Company, 2017.

Figure S5: Dynamics of actin polymerization (at 5 μM actin) when formin nucleates actin filaments, and barbed end growth with formin attached occurs at 50% of the free-ended rate (companion to Fig. **??**. Left: the fraction of free formins over time. Right: the percentage of fibers that have a formin-bound barbed end. Right: the number of fibers per unit volume. The solid lines give the total density of filaments per volume, while the dotted lines give the density of formin-bound filaments.

[2] Deb Sankar Banerjee and Shiladitya Banerjee. Emergence and maintenance of variable-length actin filaments in a limiting pool of building blocks. *Biophysical Journal*, 121(12):2436–2448, 2022.

[3] Deb Sankar Banerjee and Shiladitya Banerjee. Size regulation of multiple organelles competing for a limiting subunit pool. *PLOS Computational Biology*, 18(6):e1010253, 2022.

[4] Christopher C Beltzner and Thomas D Pollard. Pathway of actin filament branch formation by arp2/3 complex. *Journal of Biological Chemistry*, 283(11):7135–7144, 2008.

[5] Thomas A Burke, Jenna R Christensen, Elisabeth Barone, Cristian Suarez, Vladimir Sirotkin, and David R Kovar. Homeostatic actin cytoskeleton networks are regulated by assembly factor competition for monomers. *Current Biology*, 24(5):579–585, 2014.

[6] Marie-France Carlier and Shashank Shekhar. Global treadmilling coordinates actin turnover and controls the size of actin networks. *Nature Reviews Molecular Cell Biology*, 18(6):389–401, 2017.

[7] Fung-Yi Chan, Ana M Silva, Joana Saramago, Joana Pereira-Sousa, Hailey E Brighton, Marisa Pereira, Karen Oegema, Reto Gassmann, and Ana Xavier Carvalho. The arp2/3 complex
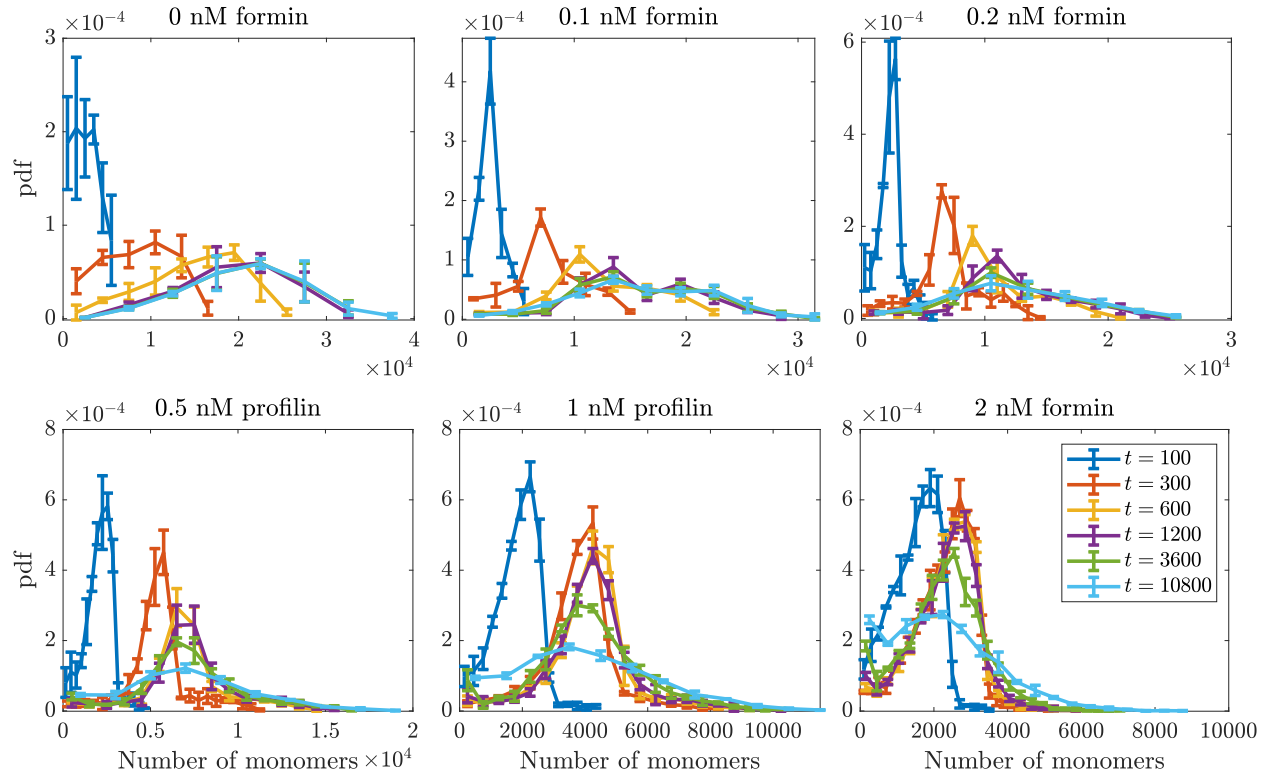
Figure S6: Length distribution for actin filaments (5 μM actin) in simulations with formin of varying concentrations. We show the distributions of fiber sizes (in terms of the number of monomers) at six time points as indicated in the legend.
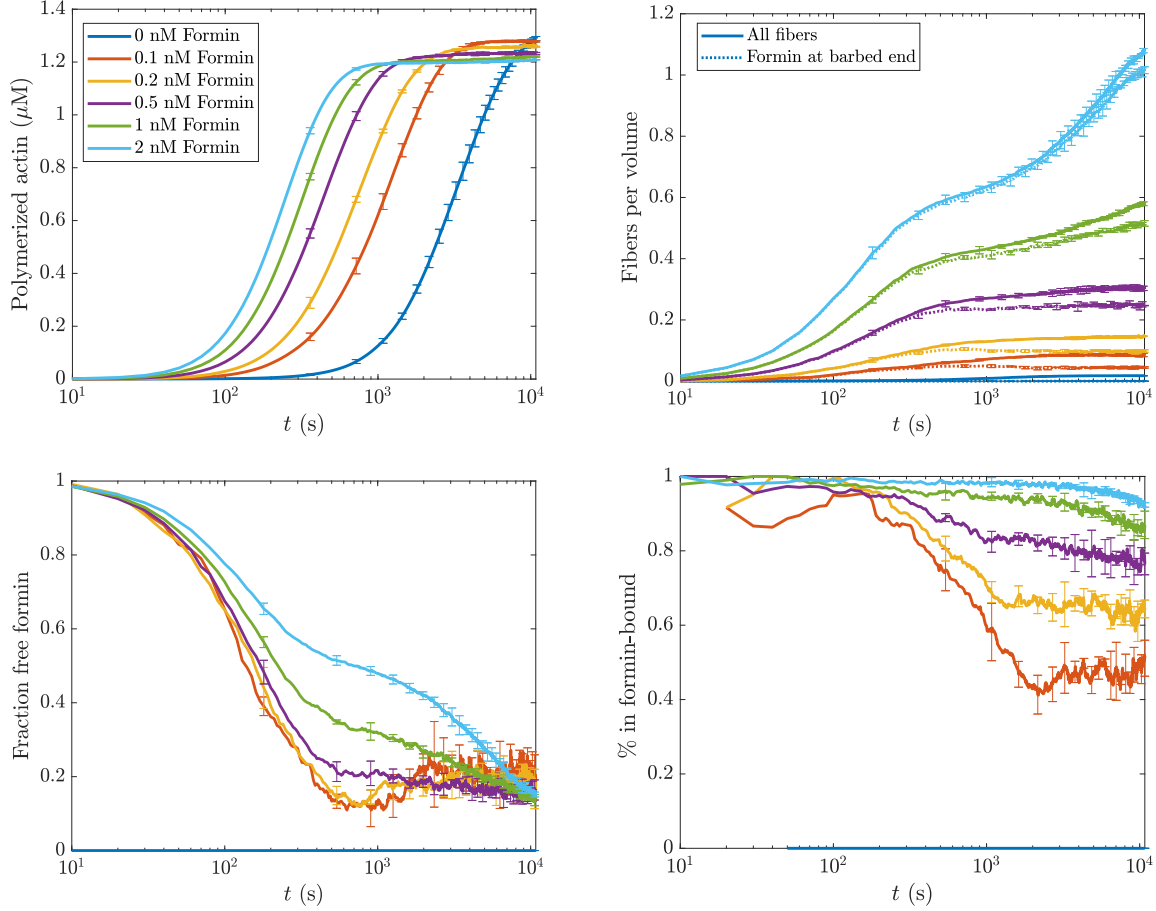
Figure S7: Dynamics of actin polymerization (at 1.5 μM actin) when formin nucleates actin filaments, and barbed end growth with formin attached occurs at 50% of the free-ended rate. Top left: the concentration of free actin monomers over time. The colors correspond to different formin concentrations. Top right: the number of fibers per unit volume. The solid lines give the total density of filaments per volume, while the dotted lines give the density of formin-bound filaments. Bottom left: the fraction of free formins over time. Right: the percentage of fibers that have a formin-bound barbed end. Bottom right: the number of fibers per unit volume. The solid lines give the total density of filaments per volume, while the dotted lines give the density of formin-bound filaments. The dynamics are similar to 5 μM actin, except that the equilibrium of the formin reaction is slower for higher formin densities.
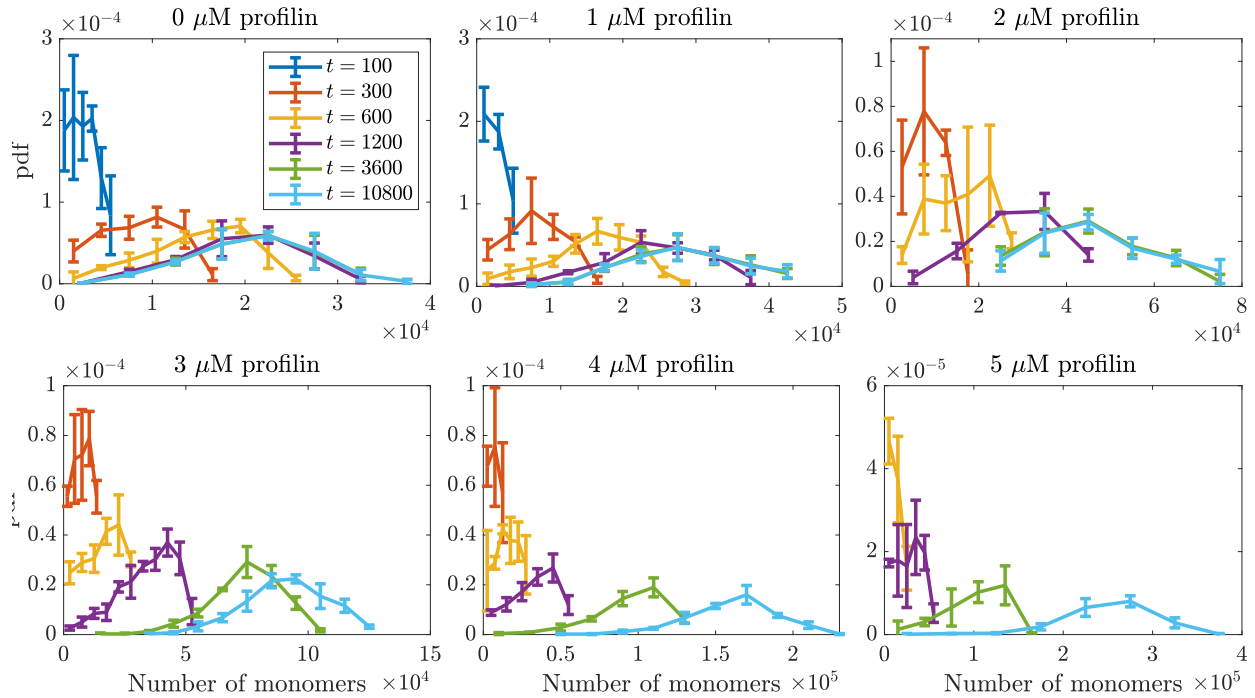
Figure S8: Dynamics of actin polymerization (at 5 μM) with profilin. Fiber length distributions over time for 2 μM profilin (left), 3 μM profilin (middle), and 4 μM profilin (right).

prevents excessive formin activity during cytokinesis. *Molecular biology of the cell*, 30(1):96–107, 2019.

[8] Aravind Chandrasekaran, Edward Giniger, and Garegin A Papoian. Nucleation causes an actin network to fragment into multiple high-density domains. *Biophysical Journal*, 121(17):3200–3212, 2022.

[9] Joseph Fass, Chi Pak, James Bamburg, and Alex Mogilner. Stochastic simulation of actin dynamics reveals the role of annealing and fragmentation. *Journal of theoretical biology*, 252(1):173–183, 2008.

[10] Daniel T Gillespie. Stochastic simulation of chemical kinetics. *Annu. Rev. Phys. Chem.*, 58:35–55, 2007.

[11] Elizabeth S Harris, Fang Li, and Henry N Higgs. The mouse formin, frlα, slows actin filament barbed end elongation, competes with capping protein, accelerates polymerization from monomers, and severs filaments. *Journal of Biological Chemistry*, 279(19):20076–20087, 2004.

[12] Jifeng Hu, Anastasios Matzavinos, and Hans G Othmer. A theoretical approach to actin filament dynamics. *Journal of Statistical Physics*, 128(1-2):111–138, 2007.

[13] David R Kovar, Elizabeth S Harris, Rachel Mahaffy, Henry N Higgs, and Thomas D Pollard. Control of the assembly of atp-and adp-actin by formins and profilin. *Cell*, 124(2):423–435, 2006.

[14] Fang Li and Henry N Higgs. The mouse formin mdia1 is a potent actin nucleation factor regulated by autoinhibition. *Current biology*, 13(15):1335–1340, 2003.

[15] James Liman, Carlos Bueno, Yossi Eliaz, Nicholas P Schafer, M Neal Waxham, Peter G Wolynes, Herbert Levine, and Margaret S Cheung. The role of the arp2/3 complex in shaping the dynamics and structures of branched actomyosin networks. *Proceedings of the National Academy of Sciences*, 117(20):10825–10831, 2020.

[16] Sophie G Martin, W Hayes McDonald, John R Yates, and Fred Chang. Tea4p links microtubule plus ends with the formin for3p in the establishment of cell polarity. *Developmental cell*, 8(4):479–491, 2005.

[17] Shane G McInally, Jane Kondev, and Bruce L Goode. Scaling of subcellular actin structures with cell length through decelerated growth. *Elife*, 10:e68424, 2021.

[18] Shane G McInally, Alexander JB Reading, Aldric Rosario, Predrag R Jelenkovic, Bruce Goode, and Jane Kondev. Length control emerges from cytoskeletal network geometry. *bioRxiv*, pages 2023–11, 2023.

[19] Lishibanya Mohapatra, Thibaut J Lagny, David Harbage, Predrag R Jelenkovic, and Jane Kondev. The limiting-pool mechanism fails to control the size of multiple organelles. *Cell systems*, 4(5):559–567, 2017.

[20] Qin Ni and Garegin A Papoian. Turnover versus treadmilling in actin network assembly and remodeling. *Cytoskeleton*, 76(11-12):562–570, 2019.

[21] Aditya Paul and Thomas Pollard. The role of the fh1 domain and profilin in formin-mediated actin-filament elongation and nucleation. *Current Biology*, 18(1):9–19, 2008.

[22] Aditya S Paul and Thomas D Pollard. Review of the mechanism of processive actin filament elongation by formins. *Cell motility and the cytoskeleton*, 66(8):606–617, 2009.

[23] Irina Perelroizen, Jean-Baptiste Marchand, Laurent Blanchoin, Dominique Didry, and Marie-France Carlier. Interaction of profilin with g-actin and poly (l-proline). *Biochemistry*, 33(28):8472–8478, 1994.

[24] Thomas D Pollard. Regulation of actin filament assembly by arp2/3 complex and formins. *Annu. Rev. Biophys. Biomol. Struct.*, 36:451–477, 2007.

[25] Thomas D Pollard and John A Cooper. Quantitative analysis of the effect of acanthamoeba profilin on actin filament nucleation and elongation. *Biochemistry*, 23(26):6631–6641, 1984.

[26] Aldric Rosario, Shane G McInally, Predrag R Jelenkovic, Bruce L Goode, and Jane Kondev. Universal length fluctuations of actin structures found in cells. *bioRxiv*, pages 2023–07, 2023.

[27] Aaron D Rosenbloom, Elizabeth W Kovar, David R Kovar, Leslie M Loew, and Thomas D Pollard. Mechanism of actin filament nucleation. *Biophysical Journal*, 120(20):4399–4417, 2021.

[28] Clarence E Schutt, James C Myslik, Michael D Rozycki, Nalin CW Goonesekere, and Uno Lindberg. The structure of crystalline profilin–β-actin. *Nature*, 365(6449):810–816, 1993.

[29] Shashank Shekhar, Mikael Kerleau, Sonja Kühn, Julien Pernier, Guillaume Romet-Lemonne, Antoine Jégou, and Marie-France Carlier. Formin and capping protein together embrace the actin filament in a ménage à trois. *Nature communications*, 6(1):8730, 2015.

[30] Benjamin A Smith, Karen Daugherty-Clarke, Bruce L Goode, and Jeff Gelles. Pathway of actin filament branch formation by arp2/3 complex revealed by single-molecule imaging. *Proceedings of the National Academy of Sciences*, 110(4):1285–1290, 2013.

[31] Cristian Suarez, Robert T Carroll, Thomas A Burke, Jenna R Christensen, Andrew J Bestul, Jennifer A Sees, Michael L James, Vladimir Sirotkin, and David R Kovar. Profilin regulates f-actin network homeostasis by favoring formin over arp2/3 complex. *Developmental cell*, 32(1):43–53, 2015.

[32] Cristian Suarez and David R Kovar. Internetwork competition for monomers governs actin cytoskeleton organization. *Nature reviews Molecular cell biology*, 17(12):799–810, 2016.

[33] Cristian Suarez, Patrick M McCall, Margaret L Gardel, and David R Kovar. When is "enough" enough? *Cell systems*, 4(5):480–482, 2017.

[34] Yi Xie, Rashmi Budhathoki, and J Todd Blankenship. Combinatorial deployment of f-actin regulators to build complex 3d actin structures in vivo. *Elife*, 10:e63046, 2021.

[35] Liyuan Xu, Lingyan Cao, Jiejie Li, and Christopher J Staiger. Cooperative actin filament nucleation by the arp2/3 complex and formins maintains the homeostatic cortical array in arabidopsis epidermal cells. *The Plant Cell*, page koad301, 2023.

[36] Mark E Zweifel, Laura A Sherer, Biswaprakash Mahanta, and Naomi Courtemanche. Nucleation limits the lengths of actin filaments assembled by formin. *Biophysical journal*, 120(20):4442–4456, 2021.